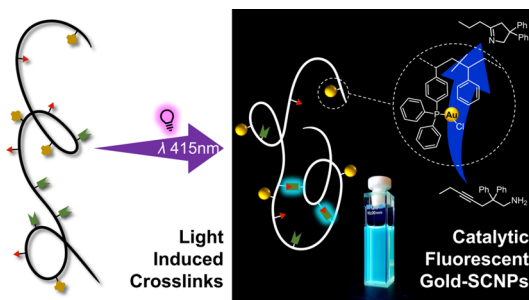


Fluorescent and Catalytically Active Single Chain Nanoparticles

Patrick H. Maag, Florian Feist, Hendrik Frisch,* Peter W. Roesky,* and Christopher Barner-Kowollik*

ABSTRACT: Fluorescent and catalytically active single chain nanoparticle (SCNP) systems allow for the visualization and tracing of the catalyst's distribution in a reaction system. We herein report a synthetic strategy to such SCNPs, generated through a photoactivated reaction at visible light ($\lambda_{\text{max}} = 415 \text{ nm}$) irradiation. Notably, the compaction reaction generates a fluorescent entity via a pro-fluorescent precursor. A polymer backbone ($M_n = 21,000 \text{ g mol}^{-1}$ and $D = 1.3$), carrying phosphine ligands for the coordination of catalytically active gold complexes and the photoreactive *ortho*-methylbenzaldehyde units and complementary alkyne moieties, was constructed based on nitroxide-mediated polymerization. The synthetic protocol entails an intermediate protection sequence for the catalyst-carrying phosphine unit to enable the installation of the cross-linking entities. The successful compaction of the SCNPs is demonstrated by a reduction in the chain's hydrodynamic volume via size exclusion chromatography and diffusion-ordered NMR spectroscopy.



INTRODUCTION

The last decade has seen substantial progress in the synthesis and application of single chain nanoparticles (SCNPs), which are currently discussed as tailored and recyclable macromolecular catalytic systems. Combining the advantages of homo- and heterogeneous catalysis, SCNPs demonstrate high turnover rates inherent to reactions in homogeneous solution with simplified isolation and recycling of the catalyst.^{1,2} SCNPs are compacted polymer chains having typical sizes between 3 and 40 nm in hydrodynamic diameter, carrying bespoke functionalities to enable applications as catalysts, sensors, nanoreactors, and in nanomedicine.³ Often, these systems take inspiration from their natural analogues,^{4,5} that is, enzymes, yet lack the precision design of catalytically active biomolecules. However, they are far easier to synthesize, typically relying on reversible deactivation radical polymerization^{6,7} to control the constituting polymer chains' length and functionality. A wide array of methodologies to generate SCNPs from linear polymer precursors has been introduced, including folding by thermal or photochemical bond formation and through intramolecular interactions such as (reversible) hydrogen bonding. The incorporated functionalities include metal complexes (including those affecting the intramolecular cross-linking reaction), luminescent entities, biologically active small molecules, or chlorine functionalities (employing SCNPs as multifunctional initiator for atom transfer radical polymerization).^{3,8,9} Our team has exploited photochemical reactions to compact single polymer chains using photochemically generated *ortho*-quinodimethanes that serve as [4 + 2] cycloaddition intermediates and highly reactive 1,3-dipoles such as nitrile imines.^{10,11} In the confined environments afforded by solvated, coiled polymer chains, the quantum efficiency of many

bimolecular photochemical processes increases dramatically, thus rendering photochemical approaches to SCNP design highly efficient.^{12,13} In addition to photochemical SCNP synthesis, photoluminescent properties of SCNPs allow monitoring of the cross-linking reactions and tracking of SCNP distributions, enabling imaging applications.^{14–17} Similarly, SCNP systems have been shown to be effective catalysts allowing the control of the solubility of the polymer backbone, which gives the opportunity to recycle the catalyst or increase the turnover frequency (TOF).^{18–22} Herein, we introduce a type of SCNP that fuses both fluorescence and catalytic activity, thus enabling the visualization of the catalyst in the reaction solution upon light excitation (Figure 1).

Photochemically induced [4 + 2] cycloadditions can be achieved by photoenolization of *o*MBA and subsequent Diels–Alder reaction with electron-deficient dienophiles. Mechanistically, the 1,5-hydrogen atom transfer taking place on the triplet manifold leads to a (Z)-enol, constituting a highly reactive diene.^{23–25} When alkynes are used as dienophiles, the initially formed non-fluorescent 1,4-dihydro-1-naphthole cycloadduct can be quantitatively converted to the respective fluorescent naphthalene via E1-elimination in the presence of catalytic amounts of acid.

We herein follow a photochemical strategy toward SCNPs utilizing the [4 + 2] cycloaddition to cross-link the polymer

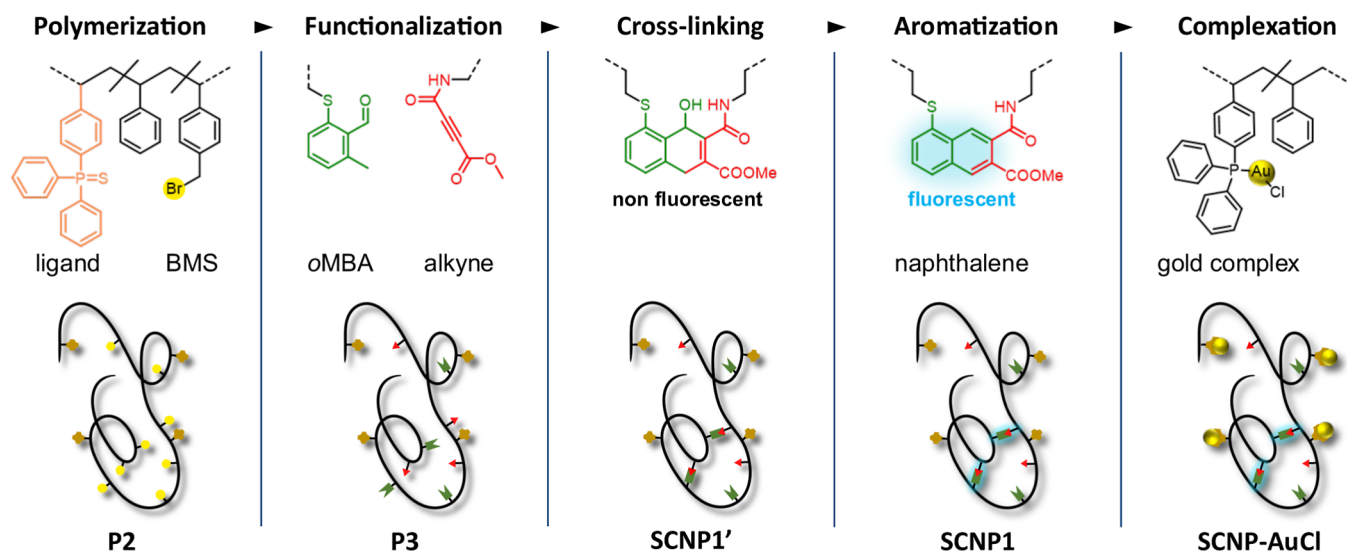


Figure 1. Overview of the SCNP synthesis in four steps. Polymerization and exchange reaction affording a styrene-based copolymer containing the $S=PPh_2Sty$ (orange) ligand and bromomethylstyrene (BMS, yellow), followed by the post-functionalization with an *ortho*-methylbenzaldehyde (*o*MBA) (green) and an alkyne (red), which are utilized to fold the polymer chain into SCNPs with fluorescent naphthalene cross-links (light blue) in the third step. In the final step, the phosphine ligands are coordinated with a catalytically active gold complex (metallic yellow).

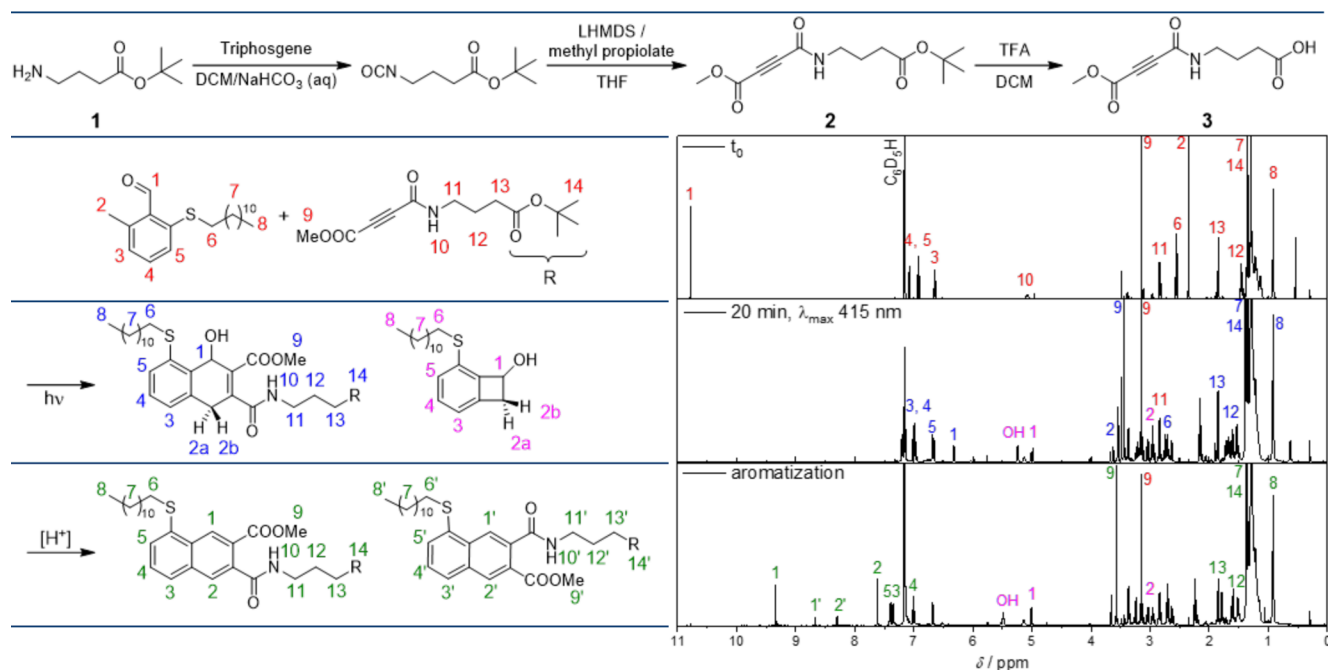


Figure 2. Top: Synthesis of 4-(4-methoxy-4-oxobut-2-ynamido)butanoic acid (**3**) starting with *tert*-butyl 4-aminobutanoate (**1**). Left: Photoreaction of *o*MBA with the alkyne (**2**) in benzene (red numbers), initially leading to the non-fluorescent 1,4-dihydro-1-naphthole (blue numbers) and benzocyclobutane as side product (pink numbers), resulting in two regioisomers of the fluorescent naphthalene through an E1-elimination (green numbers). Right: Reaction monitoring via 1H NMR spectroscopy in benzene- d_6 . The top spectrum was recorded prior to the irradiation. The middle spectrum was obtained after 20 min of irradiation at $\lambda_{max} = 415$ nm. The bottom spectrum was recorded after the addition of *p*-TsOH.

chain into a more compact structure. The emerging naphthalene cross-links are photochemically and thermally stable fluorophores reporting the cross-linking reaction itself and allowing us to trace the resulting SCNPs in reaction vessels.²⁶ In addition, a protected phosphine ligand was introduced as a monomer during the nitroxide-mediated polymerization (NMP) and utilized to coordinate gold after SCNP formation. The phosphine was protected to avoid oxidation during the polymer synthesis. Subsequent depro-

tection allows for gold coordination. NMP is a reliable, metal-free polymerization technique to obtain a defined polymer backbone with functional groups and a high end-group fidelity, especially for styrene systems.²⁷

Gold complexes are able to catalyze a range of organic reactions such as the addition of nucleophilic heteroatoms, hydroarylation, and cycloaddition reactions, often starting with the activation of unsaturated carbon bonds by forming π -complexes.^{28–31}

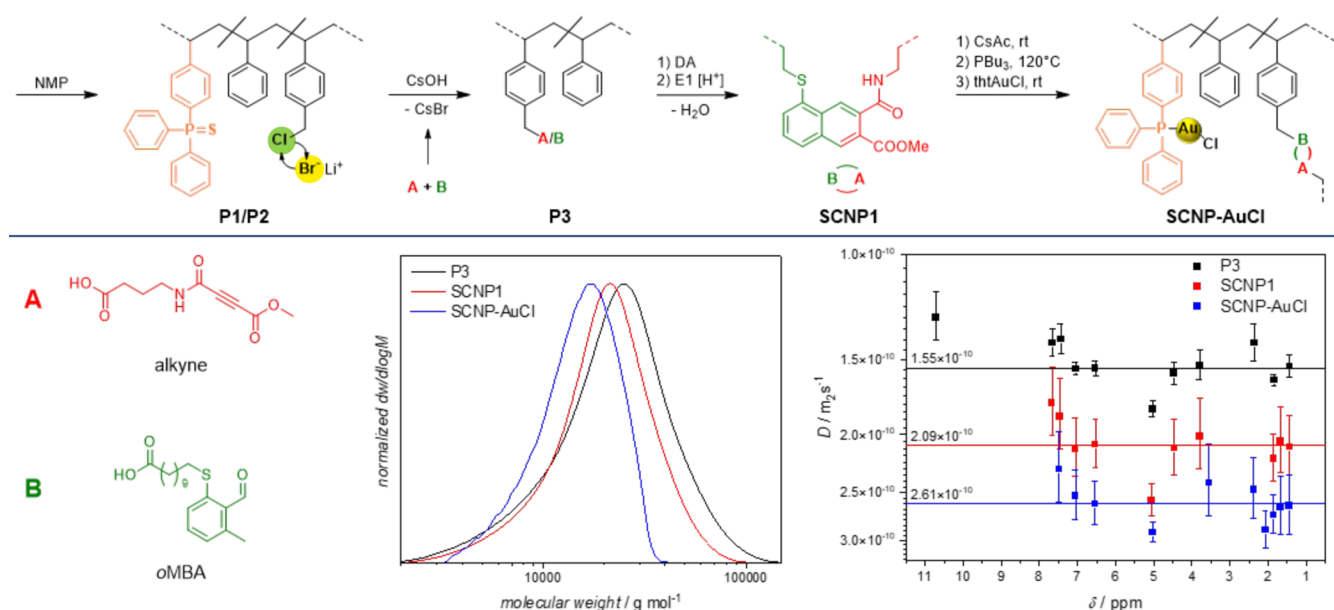


Figure 3. Overview of the detailed synthetic strategy showing the poly(Sty-*co*-BMS-*co*-S=PPh₂Sty) (**P2**) and the post-functionalization with the DA reagents, the *o*MBA, and alkyne (**P3**), as well as the resulting cross-links of **SCNP1** and the final gold(I) coordinated SCNPs (**SCNP-AuCl**). The tetrahydrofuran-SEC and diffusion coefficients, *D*, measured by DOSY of **P3**, **SCNP1**, and **SCNP-AuCl**. Both analytic methods show a significant decrease in the hydrodynamic radius after cross-linking.

RESULTS AND DISCUSSION

Herein, fluorescent SCNPs are synthesized via a photochemical cross-linking reaction of linear precursor polymers, which are subsequently equipped with catalytically active metal complexes (**SCNP-AuCl**). The synthesis commences with the generation of the polymer backbone (**P1**) containing sulfur-protected triarylphosphine (S=PPh₂Sty) along with chloromethylstyrene (CMS) units, exchanged with bromide (**P2**) to enable the following post-functionalization with a photoactive *o*MBA and an electron-deficient alkyne (**P3**). Both units react in a light-introduced Diels-Alder cycloaddition forming fluorescent cross-links, affording the SCNPs (**SCNP1**). In the final step, the triarylphosphine is used to coordinate gold(I), resulting in fluorescent and catalytically active SCNPs (**SCNP-AuCl**).

The key step in the synthesis of the SCNPs is the light-introduced [4 + 2] cycloaddition of the *o*MBA with an alkyne, leading to a fluorescent naphthalene.³² An *o*MBA thioether allows for the photoreaction to proceed under visible light irradiation ($\lambda_{\max} = 415$ nm) in agreement with earlier reports.^{33,34} Increasing the reactivity of the dienophile toward the *o*MBA aids in generating a high density of cross-links, leading to strongly folded SCNPs, yet concomitantly decreases the [4 π] electrocyclization of the *o*MBA in a side reaction. In comparison with terminal alkynes, bifunctional alkynes can carry two electron-withdrawing groups increasing the reactivity. However, to attach these alkynes to the polymer backbone, it is necessary that they carry a functional handle on one side.

The synthesis of a functional unsymmetric electron-deficient alkyne is depicted in Figure 2.³⁵ We start with *tert*-butyl 4-aminobutanoate (**1**), which was converted to an isocyanate using triphosgene and reacted further with deprotonated methyl propiolate to form an electron-deficient alkyne. The starting material already contains a carboxylic acid group in the form of a *tert*-butyl ester to allow the post-functionalization in a simple S_N2-reaction with the pendant BMS in the polymer

shown in Figure 3. The resulting *tert*-butyl-protected 4-(4-methoxy-4-oxobut-2-ynamido)butanoic acid (**2**) was used in a small molecule photoreaction to establish if it is a suitable alkyne for the Diels-Alder cycloaddition. Therefore, a reaction mixture of *o*MBA and the alkyne in deuterated benzene was irradiated at $\lambda_{\max} = 415$ nm for 20 min, and the reaction progress was monitored by ¹H NMR spectroscopy. The conversion of the *o*MBA can be observed by the disappearance of the aldehyde resonance at $\delta = 10.68$ ppm. After 20 min, the reaction reached full conversion of the *o*MBA and yields two regioisomers of the non-fluorescent 1,4-dihydro-1-naphthole. Adding a catalytic amount of acid, two regioisomers of the fluorescent naphthalene were obtained through an E1-elimination and observed by the appearance of new resonances between 7.5 and 9.5 ppm of the naphthalene.

In a side reaction, benzocyclobutane is formed during radiation via a [4 π] electrocyclization, as described in the work of Feist and Rodrigues et al.³² In comparison with conditions in SCNPs, the local concentration of the reactants is lower, and therefore, the unimolecular [4 π] electrocyclization is favored. In SCNPs, featuring high local concentrations, this reaction is disfavored in comparison with the bimolecular Diels-Alder reaction.

To introduce cross-linking units into the polymer and to use the formed SCNPs for metal coordination, a synthesis strategy considering the functional group compatibility³⁶ and stability during the consecutive polymer modification reactions is required. The synthesis commences with the NMP of styrene, CMS, and the sulfur-protected 4-(diphenylphosphino)styrene (S=PPh₂Sty), successfully avoiding side reactions between CMS and the phosphine, resulting in the formation of copolymer poly(Sty-*co*-CMS-*co*-S=PPh₂Sty) (**P1**, $M_n = 21\,000$ g mol⁻¹). The monomer composition of **P1** was determined by two methods giving similar results. First, from the conversion of the monomers during polymerization—monitored by ¹H NMR spectroscopy using an internal standard—resulting in a composition containing 18 mol % CMS and 6 mol % S=

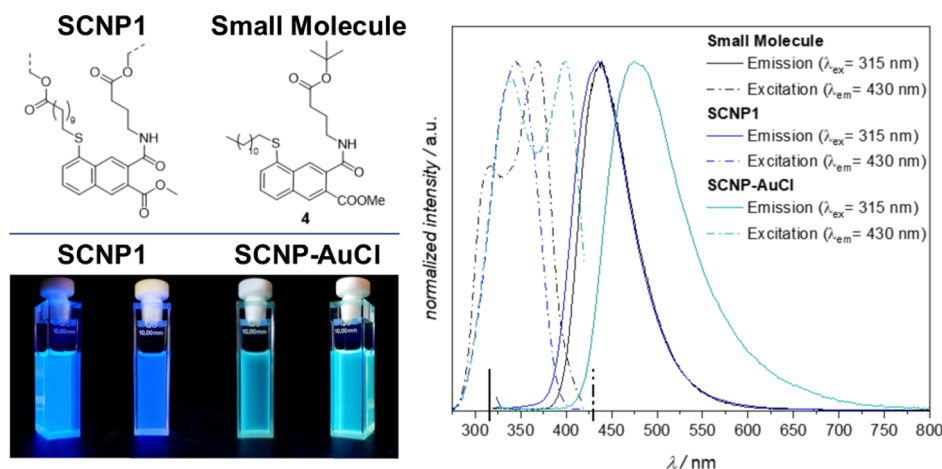


Figure 4. Fluorescence spectra of SCNP1 and gold-coordinated SCNPs (SCNP-AuCl) in comparison with the small molecule model of the fluorescent cross-links. The fluorescence spectra of the SCNP1 and the small molecules **4** show an emission and excitation band at the same wavelength, but red-shifted emission and excitation band for SCNP-AuCl.

PPh₂Sty. The second method compared the integrals of specific resonances within different functional groups of the repeating units with the integrals of the identical polymer backbone. Using the integral of the CH₂ resonance of CMS and aromatic resonance of S=PPh₂Sty allows calculating the monomer composition by comparing it with the CH-CH₂ resonance intensities of the polymer backbone. According to this method, the composition of **P1** was determined at 23 mol % CMS and 5 mol % S=PPh₂Sty (for further discussion, refer to [Supporting Information](#), section S4).

To increase the reactivity for the following post-functionalization of the CMS with the cross-linking units, the chlorine was exchanged by bromine using lithium bromide, affording poly(Sty-*co*-BMS-*co*-S=PPh₂Sty) (**P2**). The reaction of CMS to BMS was monitored by ¹H NMR spectroscopy and indicates high conversion. However, the resonances are not sufficiently separated to calculate an exact value for the conversion.

The sulfur protection group of the S=PPh₂Sty further prevents the phosphine from reacting with the alkyne during the post-functionalization of both the *o*MBA and alkyne in an esterification reaction with the BMS repeating units **P3** ($M_n = 17,000 \text{ g mol}^{-1}$, $D = 1.55 \cdot 10^{-10} \text{ m}^2 \text{ s}^{-1}$, and $R_H = 2.48 \text{ nm}$). Utilizing cesium as the counterion increases the solubility of the carboxylate in dimethylformamide and enables a faster reaction compared to sodium salts,³⁷ resulting in a conversion of 53% of BMS repeating units, monitored by ¹H NMR spectroscopy, with a ratio of *o*MBA and alkyne of 1:0.6. The post-functionalization also allows the use of highly reactive alkynes, which are not stable during NMP.

Subsequently, SCNP1 ($M_n = 15\,000 \text{ g mol}^{-1}$, $D = 2.09 \cdot 10^{-10} \text{ m}^2 \text{ s}^{-1}$, and $R_H = 1.84 \text{ nm}$) was formed by light-induced [4 + 2] cycloaddition as described above, resulting in a more compact structure. The compaction process was monitored by size exclusion chromatography (SEC) and diffusion-ordered spectroscopy (DOSY). Both analytic methods indicate a decrease in the hydrodynamic radius, R_H , after cross-linking. DOSY experiments separate ¹H NMR resonances based on their diffusion coefficient, and thus confirm that the *o*MBA (10.7 ppm) and the alkyne (3.8 ppm) are part of the polymer. The diffusion coefficients, D , increased by 34.8% after cross-linking, and consequently, the calculated hydrodynamic radius decreases, R_H .

Next, the obtained SCNPs were prepared for metal coordination. However, to prevent side reactions of the remaining functional groups such as the remaining BMS and the unreacted alkyne with the triarylphosphine or the deprotection agent (tributyl phosphine (PBU₃)), both need to be deactivated. A simple way is the esterification of BMS with cesium acetate, which concomitantly eliminates the left-over alkynes. Monitored by ¹H NMR spectroscopy, the reaction was continued until full conversion. Subsequently, the sulfur-protected triphenylphosphine units were deprotected using PBU₃ at 120 °C and monitored by ³¹P NMR showing full conversion.

The final step is the metal coordination of the deprotected SCNP. Chloro(tetrahydrothiophene)gold(I) (AuCl(tht)) was reacted with the triarylphosphine-containing SCNPs to form the desired gold(I)-decorated nanoparticles (SCNP-AuCl, $M_n = 15,000 \text{ g mol}^{-1}$, $D = 2.61 \cdot 10^{-10} \text{ m}^2 \text{ s}^{-1}$, and $R_H = 1.47 \text{ nm}$). The ³¹P NMR spectrum of the gold complex shows a resonance at 32.2 ppm (chloro(4-(diphenylphosphino)-styrene)gold(I) (AuCl-PPh₂Sty): 32.5 ppm) associated with this phosphor species and indicating full conversion. Additionally, the presence of gold complexes was confirmed via UV/vis spectroscopy, which shows an increasing absorption below 300 nm after gold complexation similar to the chloro(4-(diphenylphosphino)styrene)gold(I) complex (shown in [Figure 5](#)).

The fluorescent character of the naphthalene cross-links provides a further clear indication that the linear precursor polymer formed SCNP1 by a photoinduced Diels-Alder cycloaddition. The recorded emission and excitation fluorescence spectra are similar to the spectra of the respective non-polymer-bound small molecule **4** used as verification of their structure (shown in [Figure 4](#)).

The fluorescence spectra of SCNP-AuCl show a red shift originating from the reaction of cesium acetate with SCNP1. To investigate the cause for this red shift, **4** was subjected to similar reaction conditions used during the removal of remaining BMS groups to be able to compare the fluorescence spectra with the chemical structure, resulting in a similar, yet less pronounced, red shift compared to SCNP-AuCl. Subsequent liquid chromatography coupled mass spectrometry indicates that the ester and amid group attached at the naphthalene formed a phthalimide or an isobaric structure,

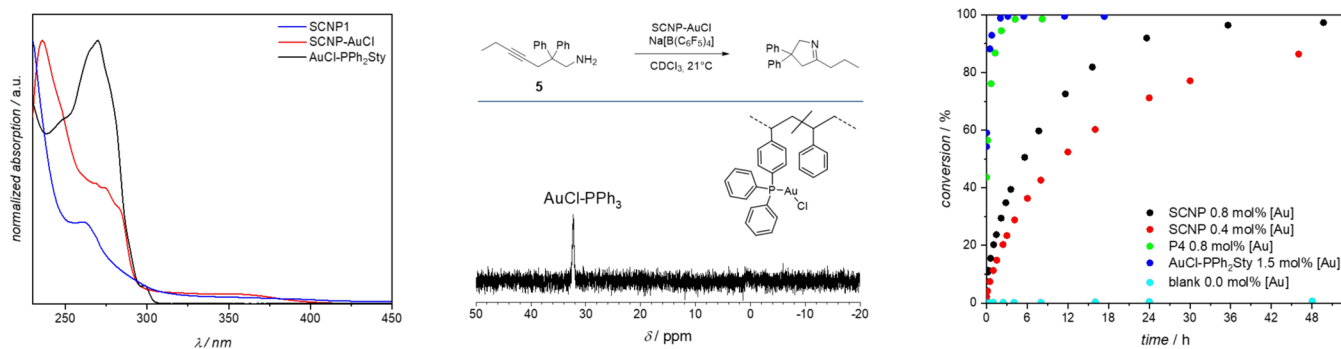


Figure 5. Left: UV/vis spectra of SCNP-AuCl show an increasing absorption band below 300 nm compared to AuCl-PPh₂Sty. Middle: The ³¹P NMR spectrum of SCNP-AuCl shows a resonance at 32.2 ppm and above it is the intramolecular hydroamination of 2,2-diphenylhept-4-yn-1-amine (**5**) utilizing SCNP-AuCl as a catalyst and Na[B(C₆F₅)₄] as cocatalysts, forming a nitrogen-containing heterocycle. Right: Kinetics of the catalyzed intramolecular hydroamination monitored by ¹H NMR spectroscopy with calculated conversion for SCNP-AuCl (0.8 mol %, 0.4 mol % [Au]), P4 (0.8 mol % [Au]), and AuCl-PPh₂Sty (1.5 mol % [Au]). Na[B(C₆F₅)₄] was used as a cocatalyst and tested in a control experiment, which showed no catalytic activity, for further discussion, refer to Supporting Information, section S5).

causing the red shift of the emission spectrum. However, this side reaction has no effect on the functionality as SCNPs or on the following catalysis (for further discussion, refer to Supporting Information, section S2).

To evidence the catalytic activity of SCNP-AuCl, we performed an intramolecular hydroamination of an amino-alkyne (**5**), which was recently published by Bohlen and Kulendran et al.³⁸ and functions as a benchmark reaction (Figure 5). Furthermore, the SCNPs were compared with linear polymer chains with incorporated AuCl-PPh₂Sty units (P4) and AuCl-PPh₂Sty complexes to study the effect of the local surroundings of the SCNPs. A cocatalyst Na[B(C₆F₅)₄] was used and tested in a control experiment, which showed no catalytic activity (for further discussion, refer to Supporting Information, section S5). The catalyst and ferrocene (internal standard) were dissolved in CDCl₃ and mixed with the cocatalyst. After dissolving, the mixture was frozen and the substrate (**5**) was added. The sample was thawed before recording the ¹H NMR spectra over time. The calculated conversion of the catalytic reaction with different concentrations of SCNP-AuCl is depicted in Figure 5. The gold fraction was calculated using ³¹P NMR spectroscopy with triphenyl phosphate as the internal standard and is based on the amount of substrate. The results demonstrate the catalytic activity of SCNP-AuCl in the intramolecular hydroamination of **5**. After 24 h, the catalysis with 0.8 mol % [Au] per substrate reaches a conversion of >90%. Also expected were the higher catalytic activities of P4 and AuCl-PPh₂Sty in comparison. However, the goal of SCNPs is not to be the faster catalysts but rather more selective—as their natural analogues, that is, enzymes. Calculating the TOF also reveals the significant increase in activity. The TOF of the unfolded polymer chain P4 (68 h⁻¹) is 13 times higher than that of the folded SCNP-AuCl (5 h⁻¹). However, by comparing SCNP-AuCl with P4 (poly(Sty-co-CMS-co-AuCl-PPh₂Sty), M_n = 20,000 g mol⁻¹), it must be considered that both polymers are not identical in molecular weight and chemical structure. In addition, the determination of the gold fraction by ³¹P NMR spectroscopy is beset with a significant error. Kinetic studies also showed that the catalytic hydroamination is a first-order reaction (for further discussion, refer to Supporting Information, section S5.5).

CONCLUSIONS

We report SCNPs that are fluorescent and catalytically active, based on linear poly(Sty-co-CMS-co-S=PPh₂Sty), containing protected phosphine moieties and CMS, functionalized with a photocaged diene and alkyne moieties, yielding a photoreactive parent polymer (P3). Irradiation with blue light (λ_{max} = 415 nm) induced a [4 + 2] cycloaddition, affording pro-fluorescent intramolecular cross-links within the compacted SCNP1. The compaction process was monitored by SEC and DOSY. Both analytical methods show a decrease in the hydrodynamic radius after cross-linking. The diffusion coefficients, *D*, increased by 34.8%. Seizing this modular SCNP platform, gold-complexes were readily introduced to enable catalysis. An intramolecular hydroamination was monitored by ¹H NMR spectroscopy using SCNP-AuCl as a catalyst showing >90% conversion after 24 h for 0.8 mol % [Au] per substrate. Importantly, the fluorescent properties of SCNP-AuCl result directly from its cross-linking and not from attachment of an additional fluorophore. Fluorescence enabling cross-linking is especially promising for the development of catalytically active SCNPs, as it allows monitoring the cross-linking reaction itself and may allow to track the distribution of the resulting SCNPs in catalytic applications through a facile fluorescence read out.

ASSOCIATED CONTENT

Supporting Information

The Supporting Information is available free of charge at <https://pubs.acs.org/doi/10.1021/acs.macromol.2c01894>.

Experimental details, additional experimental data, synthesis/characterization of polymers and SCNPs, substrate synthesis, catalytic experiments, and primary DOSY data (PDF)

AUTHOR INFORMATION

Corresponding Authors

Hendrik Frisch – Centre for Materials Science, Queensland University of Technology (QUT), Brisbane, Queensland 4000, Australia; School of Chemistry and Physics, Queensland University of Technology (QUT), Brisbane, Queensland 4000, Australia; orcid.org/0000-0001-8490-5082; Email: h.frisch@qut.edu.au

Peter W. Roesky – Institute of Inorganic Chemistry, Karlsruhe Institute of Technology (KIT), Karlsruhe 76131, Germany;

orcid.org/0000-0002-0915-3893; Email: roesky@kit.edu

Christopher Barner-Kowollik – Centre for Materials Science, Queensland University of Technology (QUT), Brisbane, Queensland 4000, Australia; School of Chemistry and Physics, Queensland University of Technology (QUT), Brisbane, Queensland 4000, Australia; Institute of Nanotechnology (INT), Karlsruhe Institute of Technology (KIT), Eggenstein-Leopoldshafen 76344, Germany; orcid.org/0000-0002-6745-0570; Email: christopher.barner-kowollik@kit.edu, christopher.barnerkowollik@qut.edu.au

Authors

Patrick H. Maag – School of Chemistry and Physics, Queensland University of Technology (QUT), Brisbane, Queensland 4000, Australia; Institute of Inorganic Chemistry, Karlsruhe Institute of Technology (KIT), Karlsruhe 76131, Germany; Institute of Nanotechnology (INT), Karlsruhe Institute of Technology (KIT), Eggenstein-Leopoldshafen 76344, Germany

Florian Feist – Institute of Nanotechnology (INT), Karlsruhe Institute of Technology (KIT), Eggenstein-Leopoldshafen 76344, Germany; orcid.org/0000-0002-2051-5488

Complete contact information is available at: <https://pubs.acs.org/10.1021/acs.macromol.2c01894>

Notes

The authors declare no competing financial interest.

ACKNOWLEDGMENTS

C.B.K. acknowledges funding from the Australian Research Council (ARC) in the form of a Laureate Fellowship (FL170100014) and support by the Deutsche Forschungsgemeinschaft (DFG) under Germany's Excellence Strategy via the Excellence Cluster "3D Matter Made to Order" (grant no. EXC-2082/1-390761711), enabling his photochemical research program and continued key support from the Queensland University of Technology (QUT). H.F. acknowledges the ARC for funding in the context of a DECRA Fellowship (DE200101096). P.W.R. acknowledges the KIT for funding. P.H.M. acknowledges KIT's Soft Matter Synthesis Laboratory for support and infrastructure for measuring fluorescence spectra.

REFERENCES

(1) Garmendia, S.; Dove, A. P.; Taton, D.; O'Reilly, R. K. Reversible ionically-crosslinked single chain nanoparticles as bioinspired and recyclable nanoreactors for N-heterocyclic carbene organocatalysis. *Polym. Chem.* **2018**, *9*, 5286–5294.
(2) Chen, R.; Berda, E. B. 100th Anniversary of Macromolecular Science Viewpoint: Re-examining Single-Chain Nanoparticles. *ACS Macro Lett.* **2020**, *9*, 1836–1843.
(3) Hanlon, A. M.; Lyon, C. K.; Berda, E. B. What is next in single-chain nanoparticles? *Macromolecules* **2016**, *49*, 2–14.
(4) Sathyan, A.; Croke, S.; Pérez-López, A. M.; de Waal, B. F. M.; Unciti-Broceta, A.; Palmans, A. R. A. Developing Pd(ii) based amphiphilic polymeric nanoparticles for pro-drug activation in complex media. *Mol. Syst. Des. Eng.* **2022**, DOI: 10.1039/d2me00173j.
(5) Deng, L.; Albertazzi, L.; Palmans, A. R. Elucidating the Stability of Single-Chain Polymeric Nanoparticles in Biological Media and Living Cells. *Biomacromolecules* **2021**, *23*, 326–338.

(6) Lyon, C. K.; Prasher, A.; Hanlon, A. M.; Tuten, B. T.; Tooley, C. A.; Frank, P. G.; Berda, E. B. A brief user's guide to single-chain nanoparticles. *Polym. Chem.* **2015**, *6*, 181–197.
(7) Corrigan, N.; Jung, K.; Moad, G.; Hawker, C. J.; Matyjaszewski, K.; Boyer, C. Reversible-deactivation radical polymerization (Controlled/living radical polymerization): From discovery to materials design and applications. *Prog. Polym. Sci.* **2020**, *111*, 101311.
(8) Mavila, S.; Eivgi, O.; Berkovich, I.; Lemcoff, N. G. Intramolecular cross-linking methodologies for the synthesis of polymer nanoparticles. *Chem. Rev.* **2016**, *116*, 878–961.
(9) Oria, L.; Aguado, R.; Pomposo, J. A.; Colmenero, J. A versatile "click" chemistry precursor of functional polystyrene nanoparticles. *Adv. Mater.* **2010**, *22*, 3038–3041.
(10) Frisch, H.; Tuten, B. T.; Barner-Kowollik, C. Macromolecular superstructures: a future beyond single chain nanoparticles. *Isr. J. Chem.* **2020**, *60*, 86–99.
(11) Claus, T. K.; Zhang, J.; Martin, L.; Hartlieb, M.; Mutlu, H.; Perrier, S.; Delaitte, G.; Barner-Kowollik, C. Stepwise Light-Induced Dual Compaction of Single-Chain Nanoparticles. *Macromol. Rapid Commun.* **2017**, *38*, 1700264.
(12) Frisch, H.; Menzel, J. P.; Bloesser, F. R.; Marschner, D. E.; Mundsinger, K.; Barner-Kowollik, C. Photochemistry in confined environments for single-chain nanoparticle design. *J. Am. Chem. Soc.* **2018**, *140*, 9551–9557.
(13) Kodura, D.; Rodrigues, L. L.; Walden, S. L.; Goldmann, A. S.; Frisch, H.; Barner-Kowollik, C. Orange-Light-Induced Photochemistry Gated by pH and Confined Environments. *J. Am. Chem. Soc.* **2022**, *144*, 6343–6348.
(14) Hoffmann, J. F.; Roos, A. H.; Schmitt, F.-J.; Hinderberger, D.; Binder, W. H. Fluorescent and Water Dispersible Single-Chain Nanoparticles: Core-Shell Structured Compartmentation. *Angew. Chem., Int. Ed.* **2021**, *60*, 7820–7827.
(15) Bajji, D. N. F.; Tran, M. V.; Tsai, H.-Y.; Kim, H.; Paisley, N. R.; Algar, W. R.; Hudson, Z. M. Fluorescent Heterotelechelic Single-Chain Polymer Nanoparticles: Synthesis, Spectroscopy, and Cellular Imaging. *ACS Appl. Nano Mater.* **2019**, *2*, 898–909.
(16) Liu, Y.; Pujals, S.; Stals, P. J. M.; Paulöhr, T.; Presolski, S. I.; Meijer, E. W.; Albertazzi, L.; Palmans, A. R. A. Catalytically Active Single-Chain Polymeric Nanoparticles: Exploring Their Functions in Complex Biological Media. *J. Am. Chem. Soc.* **2018**, *140*, 3423–3433.
(17) De-La-Cuesta, J.; González, E.; Pomposo, J. A. Advances in Fluorescent Single-Chain Nanoparticles. *Molecules* **2017**, *22*, 1819.
(18) Lambert, R.; Wirotius, A.-L.; Garmendia, S.; Berto, P.; Vignolle, J.; Taton, D. Pd(ii)-NHC coordination-driven formation of water-soluble catalytically active single chain nanoparticles. *Polym. Chem.* **2018**, *9*, 3199–3204.
(19) Xiong, T. M.; Garcia, E. S.; Chen, J.; Zhu, L.; Alzona, A. J.; Zimmerman, S. C. Enzyme-like catalysis by single chain nanoparticles that use transition metal cofactors. *Chem. Commun.* **2022**, *58*, 985–988.
(20) Chen, J.; Li, K.; Shon, J. S. L.; Zimmerman, S. C. Single-chain nanoparticle delivers a partner enzyme for concurrent and tandem catalysis in cells. *J. Am. Chem. Soc.* **2020**, *142*, 4565–4569.
(21) Huerta, E.; Stals, P. J. M.; Meijer, E. W.; Palmans, A. R. A. Consequences of Folding a Water-Soluble Polymer Around an Organocatalyst. *Angew. Chem., Int. Ed.* **2013**, *52*, 2906–2910.
(22) Rubio-Cervilla, J.; González, E.; Pomposo, J. A. Advances in Single-Chain Nanoparticles for Catalysis Applications. *Nanomaterials* **2017**, *7*, 341.
(23) Wang, J. Y. J.; Blyth, M. T.; Sherburn, M. S.; Coote, M. L. Tuning Photoenolization-Driven Cycloadditions Using Theory and Spectroscopy. *J. Am. Chem. Soc.* **2022**, *144*, 1023–1033.
(24) Sammes, P. G. Photoenolisation. *Tetrahedron* **1976**, *32*, 405–422.
(25) Segura, J. L.; Martín, N. o-Quinodimethanes: Efficient Intermediates in Organic Synthesis. *Chem. Rev.* **1999**, *99*, 3199–3246.
(26) Fan, J.; Chang, X.; He, M.; Shang, C.; Wang, G.; Yin, S.; Peng, H.; Fang, Y. Functionality-oriented derivatization of naphthalene

diimide: a molecular gel strategy-based fluorescent film for aniline vapor detection. *ACS Appl. Mater. Interfaces* **2016**, *8*, 18584–18592.

(27) Nicolas, J.; Guillaneuf, Y.; Lefay, C.; Bertin, D.; Gimes, D.; Charleux, B. Nitroxide-mediated polymerization. *Prog. Polym. Sci.* **2013**, *38*, 63–235.

(28) Widenhoefer, R. A.; Han, X. Gold-catalyzed hydroamination of C–C multiple bonds. *Eur. J. Org. Chem.* **2006**, *2006*, 4555–4563.

(29) Hashmi, A. S. K.; Hutchings, G. J. Gold catalysis. *Angew. Chem., Int. Ed.* **2006**, *45*, 7896–7936.

(30) Hashmi, A. S. K. Gold-catalyzed organic reactions. *Chem. Rev.* **2007**, *107*, 3180–3211.

(31) Dietl, M. C.; Vethacke, V.; Keshavarzi, A.; Mulks, F. F.; Rominger, F.; Rudolph, M.; Mkhali, I. A.; Hashmi, A. S. K. Synthesis of Heterobimetallic Gold (I) Palladium (II) Bis (acyclic diamino-carbene) Complexes via the Isonitrile Route. *Organometallics* **2022**, *41*, 802–810.

(32) Feist, F.; Rodrigues, L. L.; Walden, S. L.; Krappitz, T. W.; Dargaville, T. R.; Weil, T.; Goldmann, A. S.; Blinco, J. P.; Barner-Kowollik, C. Light-induced ligation of o-Quinodimethanes with Gated Fluorescence Self-reporting. *J. Am. Chem. Soc.* **2020**, *142*, 7744–7748.

(33) Feist, F.; Menzel, J. P.; Weil, T.; Blinco, J. P.; Barner-Kowollik, C. Visible light-induced ligation via o-quinodimethane thioethers. *J. Am. Chem. Soc.* **2018**, *140*, 11848–11854.

(34) Hooker, J. P.; Feist, F.; Delafresnaye, L.; Cavalli, F.; Barner, L.; Barner-Kowollik, C. On-demand acid-gated fluorescence switch-on in photo-generated nanospheres. *Chem. Commun.* **2020**, *56*, 4986–4989.

(35) Claus, T. K.; Zhang, J.; Martin, L.; Hartlieb, M.; Mutlu, H.; Perrier, S.; Delaittre, G.; Barner-Kowollik, C. Stepwise Light-Induced Dual Compaction of Single-Chain Nanoparticles. *Macromol. Rapid Commun.* **2017**, *38*, 1700264.

(36) Wong, C.-H.; Zimmerman, S. C. Orthogonality in organic, polymer, and supramolecular chemistry: from Merrifield to click chemistry. *Chem. Commun.* **2013**, *49*, 1679–1695.

(37) Dijkstra, G.; Kruizinga, W. H.; Kellogg, R. M. An assessment of the causes of the “cesium effect”. *J. Org. Chem.* **1987**, *52*, 4230–4234.

(38) Bohlen, J. L.; Kulendran, B.; Rothfuss, H.; Barner-Kowollik, C.; Roesky, P. W. Heterobimetallic Au (i)/Y (iii) single chain nanoparticles as recyclable homogenous catalysts. *Polym. Chem.* **2021**, *12*, 4016–4021.